An Apparent Violation of Microscopic Reversibility: Mechanisms for Ligand Substitution Reactions of Oxorhenium(V) Dithiolate Complexes

ARTICLE *in* JOURNAL OF THE AMERICAN CHEMICAL SOCIETY · MARCH 2007

Impact Factor: 12.11 · DOI: 10.1021/ja065428y · Source: PubMed

2 AUTHORS:

Xinzheng Yang
Chinese Academy of Sciences
55 PUBLICATIONS **969** CITATIONS
SEE PROFILE

Michael B Hall
Texas A&M University
360 PUBLICATIONS **10,301** CITATIONS
SEE PROFILE

J|A|C|S
ARTICLES
Published on Web 01/24/2007

An Apparent Violation of Microscopic Reversibility: Mechanisms for Ligand Substitution Reactions of Oxorhenium(V) Dithiolate Complexes

Xinzheng Yang and Michael B. Hall*

Contribution from the Department of Chemistry, Texas A&M University, College Station, Texas 77843-3255

Received July 27, 2006; E-mail: mbhall@tamu.edu

Abstract: The first theoretical investigation on the mechanism for ligand substitution in five-coordinate square pyramidal oxorhenium dithiolate complexes, $CH_3ReO(SCH_2C_6H_4S)-X$, has been carried out with the Perdew−Burke−Ernzerhof density functional and the Stuttgart relativistic effective-core-potential basis sets. In the mechanism proposed in the experimental kinetic studies, the entering ligand Y attacks the vacant lower axial coordinate site trans to O, and the resulting six-coordinate intermediate rearranges through a turnstile twist (a trigonal prismatic intermediate or transition state) or pentagonal pyramid to allow the leaving ligand X to exit from the same site. These workers proposed this rearrangement to avoid a violation of microscopic reversibility. The computed energy barriers in this reaction pathway show that the turnstile or pentagonal pyramidal transition states are too high in energy to make this pathway accessible. Although the vacant lower axial site in the rhenium complex is the site most easily attacked by Y, transition states for X leaving from the site cis to the attack have quite low energy barriers. Although this direct-exchange mechanism was thought to lead to a violation of microscopic reversibility, we show that these direct-exchange pathways provide low-energy routes for ligand exchange and clarify this apparent violation of microscopic reversibility. Furthermore, computed results of different entering and leaving ligand pairs are analyzed for their effect on the choice of reaction pathways. In the direct-exchange mechanism, the replacement of 4-^{t}Bu-pyridine by $PPhMe_2$ is monophasic without an intermediate, but the replacement of PPh_3 by $PPhMe_2$ is biphasic (proceeds by a two-stage pathway) and generates the observed intermediate, an isomer of product. These predictions are completely consistent with the observed experimental phenomena. The accuracy of the particular functional/basis set used for the study is compared to 10 functionals in 19 basis sets and to large basis set coupled cluster calculations on model systems.

Understanding of the mechanism for ligand substitution reactions is fundamental to all of inorganic chemistry, and, in these particular systems, it holds an important relationship to the whole cycle of oxygen-atom-transfer (OAT) reactions catalyzed by the transition metal complexes and metalloenzymes. These OAT reactions are important in a variety of enzymes such as sulfite oxidase and DMSO reductase, where Mo or W act at the catalytic centers.[1] In addition to synthetic Mo and W OAT systems,[2] oxorhenium complexes have been developed and studied extensively in recent decades.[3−5]

Lahti and Espenson[4] (LE) measured the kinetics of the ligand substitution reactions between five-coordinate oxorhenium dithiolates $CH_3ReO(SCH_2C_6H_4S)-X$ (MeReO(mtp), M−X in Scheme 1), for a variety of leaving ligands (X, mainly substituted pyridine or alkyl and aryl phosphines) and entering ligands (Y, mainly other phosphines). In many cases, they observed biphasic reactions with an apparent intermediate, M−Y*, in which the positions of CH_3 and Y have been exchanged (Scheme 2). While

Scheme 1

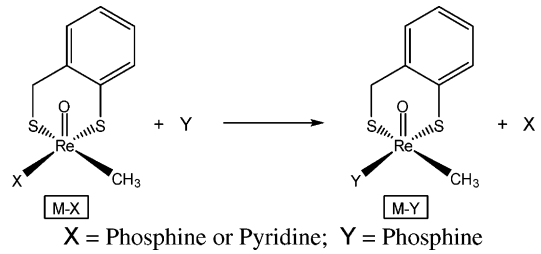

Scheme 2

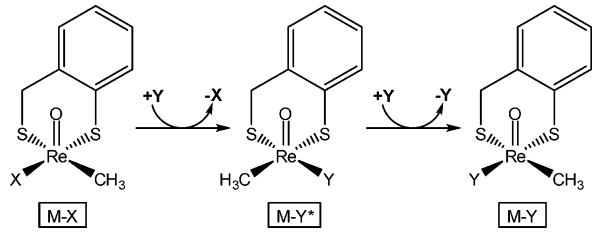

(1) (a) Hille, R. *Chem. Rev.* **1996**, *96*, 2757−2816. (b) Johnson, M. K.; Rees, D. C.; Adams, M. W. W. *Chem. Rev.* **1996**, *96*, 2817−2839. (c) Schindelin, H.; Kisker, C.; Rajagopalan, K. V. *Adv. Protein Chem.* **2001**, *58*, 47−94. (d) Brondino, C. D.; Romao, M. J.; Moura, I.; Moura, J. J. G. *Curr. Opin. Chem. Biol.* **2006**, *10*, 109−114.
(2) Enemark, J. H.; Cooney, J. J. A. *Chem. Rev.* **2004**, *104*, 1175−1200.
(3) (a) Gable, K. P. *Adv. Organomet. Chem.* **1997**, *41*, 127−161. (b) Espenson, J. H. *Chem. Commun.* **1999**, 479−488. (c) Espenson, J. H. *Adv. Inorg. Chem.* **2003**, *54*, 157−202.
(4) Lahti, D. W.; Espenson, J. H. *J. Am. Chem. Soc.* **2001**, *123*, 6014−6024.
(5) Espenson, J. H. *Coord. Chem. Rev.* **2005**, *249*, 329−341.

10.1021/ja065428y CCC: $37.00

Scheme 3

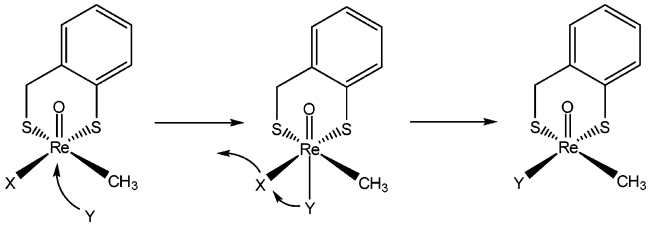

other cases showed monophasic kinetics and no detectable intermediates, LE suggested that the intermediates were not absent but disguised by a high reaction rate in one of the two stages.

In developing the mechanism for these systems, LE proposed that an incoming ligand, Y, could only enter at the vacant coordination site as other approaches would be too crowded. Microscopic reversibility then requires that the leaving ligand, X, also leave from this site. Thus, the direct-exchange of ligands as shown in Scheme 3 was eliminated from further consideration as it would appear to violate microscopic reversibility.

To avoid violating microscopic reversibility, LE proposed a mechanism that involves a rearrangement of the six-coordinate intermediate through a turnstile twist (a trigonal prismatic intermediate or transition state) or a pentagonal pyramidal structure (Scheme 4). The proposed intermediate M−Y*, an isomer of final product M−Y, was observed for some but not all ligand pairs. This mechanism is often cited as an example of the application of the principle of microscopic reversibility.[5,6]

Here, we study the mechanisms of ligand substitution reactions of these oxorhenium complexes through density functional theory[7] (DFT) calculations on the relative energies in the turnstile, pyramidal, and direct-exchange mechanisms. To have representative ligand pairs that show both monophasic and biphasic kinetics, we chose two experimentally studied systems, entering ligand Y = $PPhMe_2$ and leaving ligands X = 4-^{t}BuPy or PPh_3. Other experimentally studied pairs are close enough to these two examples that our results should be representative of the whole class of reactants. The accuracy of the methodology, density functional, and basis set was examined with simplified model systems.

Results and Discussion

Analysis of the Turnstile and Pyramidal Mechanisms. The reaction pathway and predicted relative enthalpies of the intermediates ($\Delta H°$) and transition states ($\Delta H^{\ddagger}$) for the turnstile mechanism are shown in Scheme 4 and Figure 1 for the case X = 4-^{t}BuPy and Y = $PPhMe_2$. All relative enthalpies were calculated in the gas phase at 298.15 K with complex M−X and separated Y ligand set to 0.0 kcal/mol unless otherwise noted.

While the proposed intermediates are stable enough and the barriers for ligand attack and loss are reasonable, the calculated energy barrier for the turnstile rearrangement is far too high ($\mathbf{TS_{T1}}$ = 43.3 and $\mathbf{TS_{T2}}$ = 49.6 kcal/mol) to account for the observed reaction. The optimized geometries of the stable structure of six-coordinate intermediate $\mathbf{MXY_1}$ and the transition state $\mathbf{TS_{T1}}$ are displayed in Figures 2 and 3, respectively. From $\mathbf{MXY_1}$ to $\mathbf{TS_{T1}}$, the strong bonds Re−O, Re−C, Re−N, and Re−S2 become longer, while the Re−S1 and Re−P bonds become shorter. Specifically, the largest changes are in the Re−P and Re−C bond length. The former bond (Re−P), which is very weak in the intermediate because it is trans to the strongest "trans-influence" ligand (O), becomes stronger in $\mathbf{TS_{T1}}$. However, the strong Re−C bond weakens considerably in $\mathbf{TS_{T1}}$ as it is now competing with the O for the same Re d orbital.

Scheme 4. Reaction Pathway and Computed Relative Enthalpies (kcal/mol) of the Intermediates ($\Delta H°$) and Transition States ($\Delta H^{\ddagger}$) for the Turnstile and Pyramidal Mechanisms Proposed by Lahti and Espenson[4] [a]

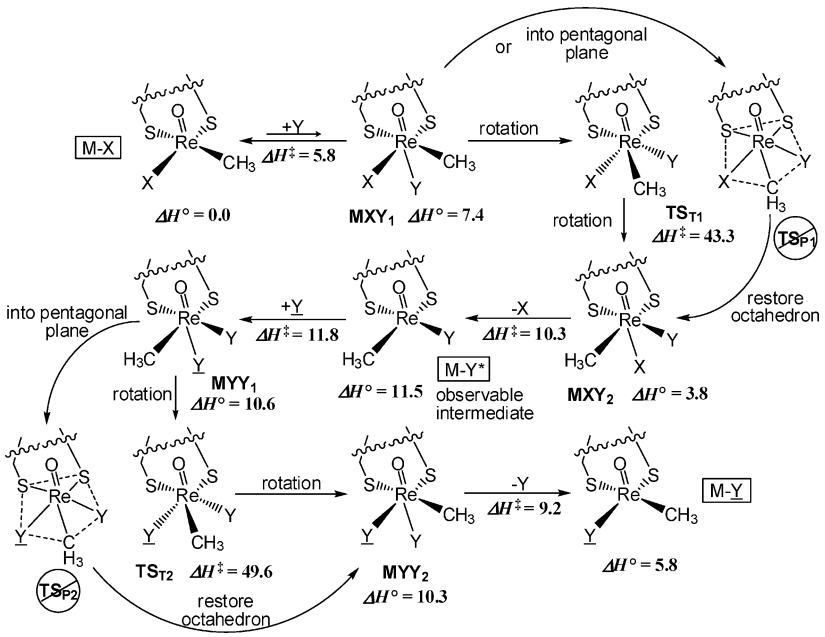

[a] X = 4-^{t}BuPy and Y = $PPhMe_2$. The initial attack of Y at the vacant coordination site (or the loss of X ligand from this site) has such a low barrier on the electronic energy surface (E_e) that the usual thermal corrections based on harmonic vibrational frequency produce a transition state enthalpy below that of six-coordinate intermediate.

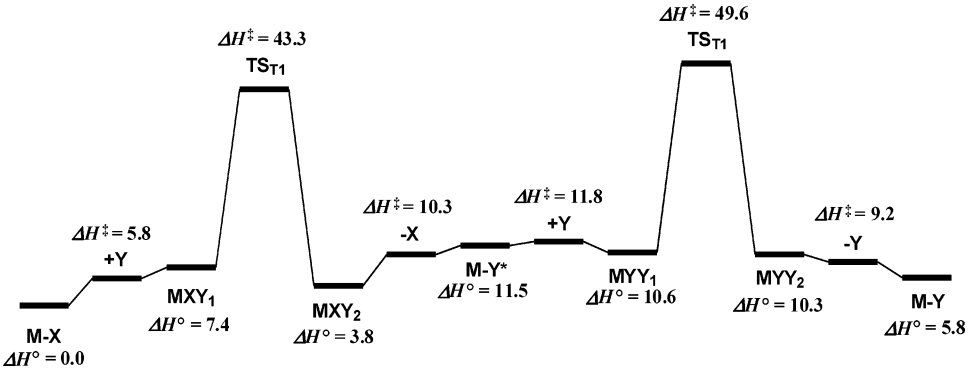

Figure 1. Computed relative enthalpies (kcal/mol) of the intermediates ($\Delta H°$) and transition states ($\Delta H^{\ddagger}$) for the turnstile mechanisms. X = 4-^{t}BuPy and Y = $PPhMe_2$.

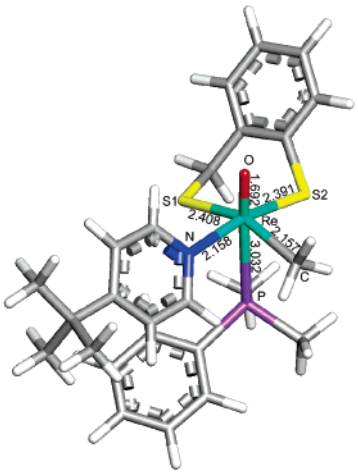

Figure 2. The stable structure of six-coordinate intermediate $\mathbf{MXY_1}$ when entering ligand Y = $PPhMe_2$ attacks the vacant lower axial coordinate site trans to O. Leaving ligand X = 4-^{t}BuPy. The dihedral of C−Re−S2−S1 is 151.5°. Unit for bond length is angstrom. First vibrational frequency is 17.14 cm^{-1}.

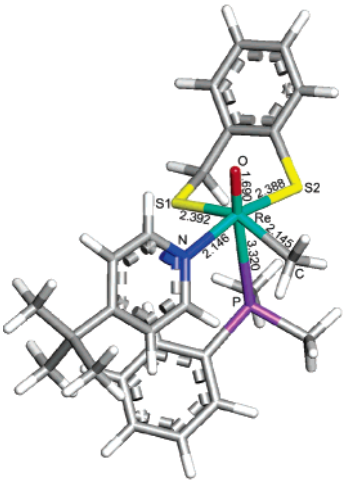

Figure 4. The structure of transition state $\mathbf{TS_{1,2a}}$ in the direct-exchange mechanism. X = 4-^{t}BuPy and Y = $PPhMe_2$. The dihedral of C−Re−S2−S1 is 146.8°. Unit for bond length is angstrom. Imaginary frequency is −34.86 cm^{-1}.

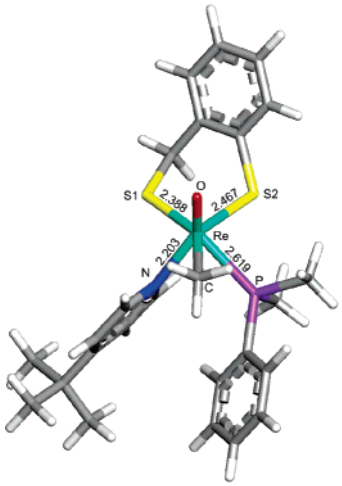

Figure 3. The structure of the transition state $\mathbf{TS_{T1}}$ in the turnstile mechanism. X = 4-^{t}BuPy and Y = $PPhMe_2$. The dihedral of C−Re−S1−S2 is 175.7°. Unit for bond length is angstrom. Re−O bond length is 1.723 Å. Re−C bond length is 2.274 Å. Imaginary frequency is −79.13 cm^{-1}.

All of these changes make the transition state $\mathbf{TS_{T1}}$ high energy. All attempts to find a stationary point (intermediate, transition state, or higher-order saddle point) required for any alternative rearrangement failed. The proposed pentagonal-pyramidal structures were higher in energy than $\mathbf{TS_{T1}}$ and unstable (not stationary points) and collapsed to the turnstile transition state during further optimizations.

Direct-Exchange Mechanism. Following our initial surprise that the turnstile and pentagonal-pyramidal mechanisms were too high in energy to explain the observed reaction and our failure to find any other rearrangement, we began an examination of the direct-exchange pathway (Scheme 3) and found low-energy pathways by this route. On the basis of further exploration of related pathways, we determined the complete mechanism as shown in Scheme 5 for X = 4-^{t}BuPy and Y = $PPhMe_2$, and selected values for the ligand pair X = PPh_3 and Y = $PPhMe_2$ are shown in square brackets.

Scheme 5 shows three reaction pathways **a**, **b**, and **c** leading to the final product M−Y, **3a**, in this direct-exchange mechanism. In the first pathway, **a**, the entering ligand Y attacks the five-coordinate oxorhenium compound M−X, **1**, from the vacant lower axial position through a very low-energy barrier $\mathbf{TS_{1,2a}}$ (5.8 kcal/mol, Figure 4) to form the six-coordinate intermediate **2a**. Next, the ligand X leaves the rhenium atom directly, and Y

(6) (a) McPherson, L. D.; Drees, M.; Khan, S. I.; Strassner, T.; Abu-Omar, M. M. *Inorg. Chem.* **2004**, *43*, 4036−4050. (b) Shan, X.; Espenson, J. H. *Dalton Trans.* **2003**, 3612−3616.
(7) (a) Hohenberg, P.; Kohn, W. *Phys. Rev.* **1964**, *136*, B864−871. (b) Kohn, W.; Sham, L. J. *Phys. Rev.* **1965**, *140*, A1133−1138.

Scheme 5. Reaction Pathway and Calculated Relative Enthalpies (kcal/mol) of the Intermediates ($\Delta H°$) and Transition States ($\Delta H^{\ddagger}$) for the Direct-Exchange Mechanisms for X = 4-^{t}BuPy and Y = $PPhMe_2$ and for Selected Values of X = PPh_3 and Y = $PPhMe_2$ in Square Brackets[a]

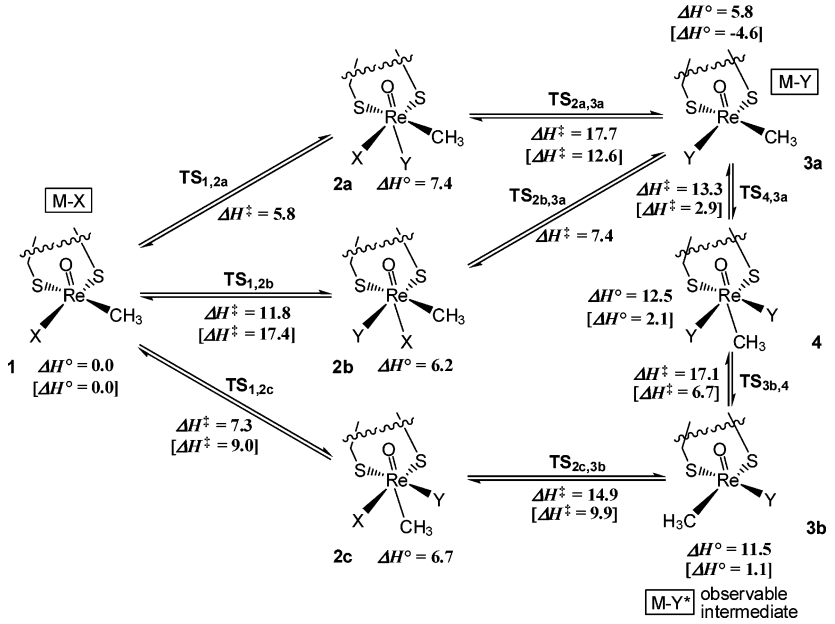

[a] The initial attack of Y at the vacant coordination site (or the loss of X ligand from this site) has such a low barrier on the electronic energy surface (E_e) that the usual thermal corrections based on harmonic vibrational frequency produce a transition state enthalpy below that of six-coordinate intermediate.

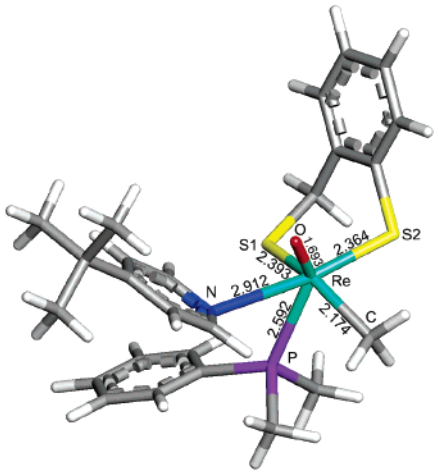

Figure 5. The structure of the transition state **$TS_{2a,3a}$** in the direct-exchange mechanism. X = 4-^{t}BuPy and Y = $PPhMe_2$. The dihedral of C−Re−S2−S1 is 142.7°. The dihedral of N−Re−S1−S2 is 169.0°. Unit for bond length is angstrom. Imaginary frequency is −62.27 cm^{-1}.

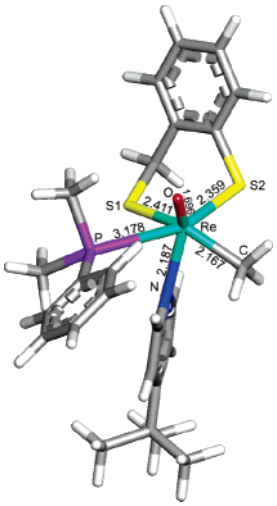

Figure 6. The structure of the transition state **$TS_{1,2b}$** in the direct-exchange mechanism. X = 4-^{t}BuPy and Y = $PPhMe_2$. The dihedral of C−Re−S2−S1 is 147.1°. Unit for bond length is angstrom. Imaginary frequency is −62.92 cm^{-1}.

moves up from the lower axial position to replace X in the basal site through a single, somewhat higher energy transition state **$TS_{2a,3a}$** (17.7 kcal/mol, Figure 5).

The second reaction pathway, **b**, is the reverse of pathway **a**, and the difference in energies on the two pathways arises because X ≠ Y. In pathway **b**, Y attacks from above X, and X moves down to the lower axial position to form the six-coordinate intermediate **2b** via **$TS_{1,2b}$** (11.8 kcal/mol, Figure 6). Next, X leaves the Re atom directly from the lower axial position through the transition state **$TS_{2b,3a}$** (7.4 kcal/mol), and Y remains at the basal site formerly occupied by X.

It was expectations about this latter pathway, **b**, that led LE to propose a mechanism that avoided the direct-exchange. Because Y would have to attack from the more crowded side (as opposed to pathway **a** where Y attacks at the vacant site), they made the apparently quite reasonable assumption that pathway **b** would be much too high in energy to be part of the reaction mechanism. Although the barrier for attack at the more crowded position (**$TS_{1,2b}$**, 11.8 kcal/mol, Figure 6) is higher than the barrier for attack at the vacant site (**$TS_{1,2a}$**, 5.8 kcal/mol, Figure 4), the former is still a relatively low-energy process, and its existence explains how direct-exchange maintains microscopic reversibility. Interestingly, for the pair of ligands X = 4-^{t}BuPy and Y = $PPhMe_2$, pathway **b** actually provides a lower overall barrier than pathway **a** as ligand loss from the six-coordinate intermediate **2a** and subsequent rearrangement on pathway **a** through **$TS_{2a,3a}$** (17.7 kcal/mol, Figure 5) is even more "crowded". The energy of **$TS_{2a,3a}$** is higher than that of **$TS_{1,2b}$** simply because the 4-^{t}BuPy ligand has stronger interaction

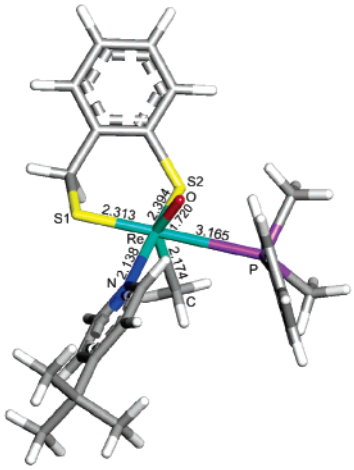

Figure 7. The structure of the transition state $\mathbf{TS_{1,2c}}$ in the direct-exchange mechanism. X = 4-^{t}BuPy and Y = $PPhMe_2$. The dihedral of P−Re−S2−S1 is 178.8°. The dihedral of N−Re−S1−S2 is 161.9°. Unit for bond length is angstrom. Imaginary frequency is −61.13 cm^{-1}.

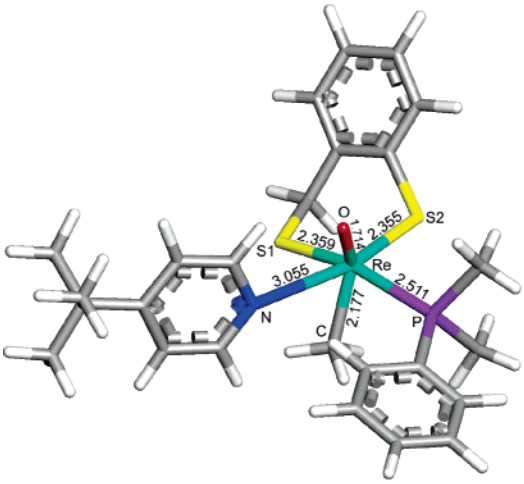

Figure 8. The structure of the transition state $\mathbf{TS_{2c,3b}}$ in the direct-exchange mechanism. X = 4-^{t}BuPy and Y = $PPhMe_2$. The dihedral of P−Re−S2−S1 is 159.8°. The dihedral of N−Re−S1−S2 is 171.6°. Unit for bond length is angstrom. Imaginary frequency is −46.12 cm^{-1}.

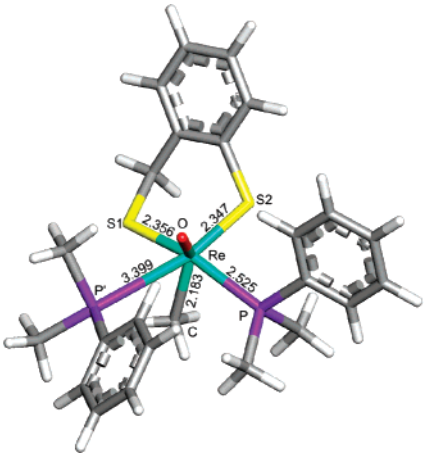

Figure 9. The structure of the transition state $\mathbf{TS_{3b,4}}$ in the direct-exchange mechanism. X = 4-^{t}BuPy and Y = $PPhMe_2$. The dihedral of P−Re−S2−S1 is 159.3°. The dihedral of P′−Re−S1−S2 is 169.6°. Unit for bond length is angstrom. Re−O bond length is 1.723 Å. Imaginary frequency is −56.27 cm^{-1}.

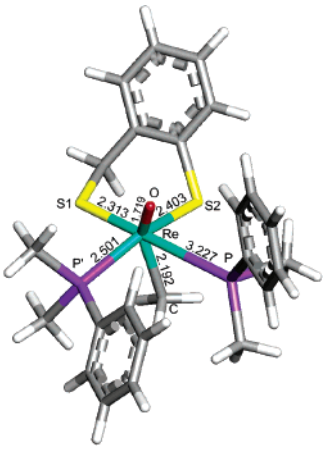

Figure 10. The structure of the transition state $\mathbf{TS_{4,3a}}$ in the direct-exchange mechanism. X = 4-^{t}BuPy and Y = $PPhMe_2$. The dihedral of P−Re−S2−S1 is 176.9°. The dihedral of P′−Re−S1−S2 is 162.8°. Unit for bond length is angstrom. Imaginary frequency is −58.41 cm^{-1}.

with the Re atom than the $PPhMe_2$ ligand. The Re−P bond is about 0.6 Å shorter, but the Re−N bond length is about 0.8 Å larger in $\mathbf{TS_{2a,3a}}$ than those in $\mathbf{TS_{1,2b}}$ (compare Figure 5 and Figure 6). Other Re bonds have only very few changes. To this point, our proposed reaction mechanism from reactant **1** to observed product **3a** does not produce the apparent intermediate that was observed by LE. So, how does this observed species, a less stable isomer of the product in which CH_3 and Y have exchanged places (M−Y* and **3b** in Scheme 5), actually form, and what is its relationship to our newly proposed mechanism? The route through **3b** is shown as the third reaction pathway, **c**, in Scheme 5.

In pathway **c**, the ligand Y attacks the reactant M−X, **1**, from the right, above, and near the CH_3 position, while the CH_3 moves down to the lower axial position to form the six-coordinate intermediate **2c** via $\mathbf{TS_{1,2c}}$ (7.3 kcal/mol, Figure 7). In the second step, X leaves the Re atom directly and CH_3 moves up to the original basal position of X through the transition state $\mathbf{TS_{2c,3b}}$ (14.9 kcal/mol, Figure 8) to generate the isomer M−Y* (**3b** in Scheme 5). In the third step, another Y ligand attacks M−Y* from left, above, and near CH_3 to form a six-coordinate intermediate **4** through the transition state $\mathbf{TS_{3b,4}}$ (17.1 kcal/mol, Figure 9). Next, in the final step, the Y ligand on the right leaves the Re atom directly, while CH_3 moves up simultaneously to its original position through the transition state $\mathbf{TS_{4,3a}}$ (13.3 kcal/mol, Figure 10) to form the final product M−Y (**3a** in Scheme 5). Because all reactions in the direct-exchange mechanism are completely reversible, M−Y* can be generated not only from the reactant M−X through $\mathbf{TS_{1,2c}}$ and $\mathbf{TS_{2c,3b}}$, but also from the product M−Y through $\mathbf{TS_{4,3a}}$ and $\mathbf{TS_{3b,4}}$.

Ligand Effects (Monophasic versus Biphasic Kinetics). For the ligand pair X = 4-^{t}BuPy and Y = $PPhMe_2$, the $\Delta H^{\ddagger}$ of $\mathbf{TS_{1,2b}}$ is about 3 and 5 kcal/mol lower than those of $\mathbf{TS_{2c,3b}}$ and $\mathbf{TS_{3b,4}}$, respectively. Thus, the generation of product M−Y through pathway **b** would be much faster than the generation of the isomer M−Y* through pathway **c** from either reactant or product. In this case, only small amounts of M−Y* will be produced, and the reaction will appear monophasic. In agreement with our prediction, LE did not observe an intermediate for this particular ligand pair. However, if we change the leaving ligand X to a triphenyl phosphine (PPh_3) and keep the entering ligand Y as $PPhMe_2$, the two high-energy barriers on pathway **c**, $\mathbf{TS_{2c,3b}}$

Table 1. Calculated Dissociation Energies for the Re−P Bond between MeReO(mtp) and PMe_3 with the B3LYP Functional and Various Basis Sets

no.	Re outermost 15 electrons	ECP for Re inner 60 electrons	other atoms	D_e (kcal/mol)
BS01	LANL2DZ	LANL2DZ ECP	LANL2DZ	33.39
BS02	LANL2DZ & Couty-Hall 6p	LANL2DZ ECP	LANL2DZ & dp	33.52
BS03	LANL2DZ & Couty-Hall 6p & f	LANL2DZ ECP	LANL2DZ	33.72
BS04	LANL2DZ & Couty-Hall 6p & f	LANL2DZ ECP	LANL2DZ & dp	33.42
BS05	LANL2DZ & Couty-Hall 6p & f	LANL2DZ ECP	cc-pVTZ	32.85
BS06	QZVPP	LANL2DZ ECP	6-311++G(3df,3pd)	33.77
BS07	QZVPP	LANL2DZ ECP	6-311G	32.93
BS08	QZVPP	LANL2DZ ECP	LANL2DZ & dp	32.27
BS09	TZVPP	LANL2DZ ECP	LANL2DZ & dp	31.94
BS10	QZVPP	Stuttgart RSC 1997 ECP	6-311G	32.77
BS11	QZVPP	Stuttgart RSC 1997 ECP	LANL2DZ & dp	31.58
BS12	TZVPP	Stuttgart RSC 1997 ECP	6-311G	32.67
BS13	TZVPP	Stuttgart RSC 1997 ECP	LANL2DZ & dp	31.17
BS14	Stuttgart RSC 1997	Stuttgart RSC 1997 ECP	LANL2DZ & dp	31.91
BS15	Stuttgart RSC 1997 & f	Stuttgart RSC 1997 ECP	LANL2DZ & dp	31.79
BS16	Stuttgart RSC 1997 & f	Stuttgart RSC 1997 ECP	Stuttgart RLC ECP	33.52
BS17	Stuttgart RSC 1997 & 2f1g	Stuttgart RSC 1997 ECP	Stuttgart RLC ECP	32.34
BS18	ZORA TZ2P all-electron	ZORA TZ2P all-electron	ZORA TZ2P all-electron	31.34
BS19	ZORA QZ4P all-electron	ZORA QZ4P all-electron	ZORA QZ4P all-electron	30.52

(9.9 kcal/mol) and $\mathbf{TS_{3b,4}}$ (6.7 kcal/mol), have decreased in energy enough to be below those on pathway **a** and **b**, $\mathbf{TS_{1,2b}}$ (17.4 kcal/mol) and $\mathbf{TS_{2a,3a}}$ (12.6 kcal/mol), respectively. Now, pathway **c** has the lowest energy barrier, and isomer M−Y* will be generated first as an intermediate through $\mathbf{TS_{2c,3b}}$; then, the final product M−Y will be produced from M−Y* through $\mathbf{TS_{3b,4}}$. These theoretical results are also consistent with the observed phenomena for this other ligand set. Incidentally, Y attacking **3b** or **3a** produces no new species, but would provide routes to exchange free and bound Y.

Concluding Remarks

Different combinations of basis sets and density functionals were tested for the dissociation energy between oxorhenium compounds and phosphine ligands, and, on the basis of these results, the double-ζ quality Stuttgart basis sets and PBE density functional were selected for the investigation on mechanisms for ligand substitution in five-coordinate oxorhenium dithiolate, $CH_3ReO(SCH_2C_6H_4S)-X$, complexes. The calculations demonstrate that both the turnstile and the pentagonal-pyramidal rearrangement of the six-coordinate complexes are too high in energy to be accessed. Furthermore, the calculations show that these ligand substitution reactions proceed through a direct-exchange pathway that does not violate microscopic reversibility. Although the vacant axial position is the most easily attacked site, the alternative site of attack, which is required by microscopic reversibility, is still quite low in energy. In the direct-exchange mechanism, different entering and leaving ligand pairs will select different possible reaction pathways. Consistent with the experiments, our pathway displays monophasic kinetics with no intermediate, while the other pathway displays biphasic kinetics and an intermediate.

Computational Details

Because the actual molecular system contains large ligands and a third-transition-row metal, rhenium, DFT calculations with relativistic effect-core-potential (ECP) basis sets are the only suitable theoretical model that can balance the precision and computational cost. Recent developments in both ab initio theory and DFT provide a wide variety of basis sets and density functionals. There is no a priori criterion for judging which basis set and density functional combination is most appropriate for a given system. Thus, we need some experience in related systems, or one needs to examine the system with a variety of basis sets and functionals. Because the essence of ligand substitution is breaking and forming chemical bonds between the metal and ligands, we selected the dissociation energy (D_e) between the Re atom and a phosphine ligand (M−X → M + X) as the physical quantity to examine in searching for a suitable theoretical model. In particular, we will study the reaction shown in Scheme 6.

Scheme 6

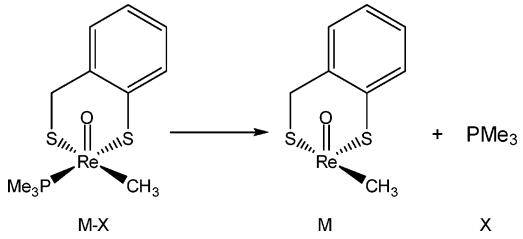

Table 2. Calculated Dissociation Energies between MeReO(mtp) and PMe_3 with BS17 and Various Density Functionals

functional	D_e (kcal/mol)
PW91	36.39
PBE	35.67
PBE1PBE	40.89
OPBE	28.13
OLYP	23.42
BLYP	26.26
B3LYP	32.34
B3PW91	35.61
BHandHLYP	37.74
MPW91PW91	38.42

Effect of Basis Set. Nineteen basis sets (BS01−BS19) were examined with the popular B3LYP functional[8] to determine the effect of basis sets on the $D_e = E_{MX} - E_M - E_X$. The geometric structures of M, X, and M−X were optimized separately for each basis set to obtain their total electronic energies E. The 19 results for D_e are listed in Table 1. Calculations were performed by using Gaussian 03[9] for BS01−BS17 and ADF 2005[10] for BS18 and BS19.

Basis sets 1−17 were constructed using various combinations of Gaussian-type basis sets for Re and other atoms. For the outermost 15 electrons (semi-core, $5s^25p^6$, and valence, $5d^56s^2$) of Re, basis sets of

(8) Becke, A. D. *J. Chem. Phys.* **1993**, *98*, 5648−5652.

Table 3. Calculated Dissociation Energies between $HReO(SH)_2$ and PH_3 with the PBE Functional and Various Basis Sets

no.	Re outermost 15 electrons	ECP for Re inner 60 electrons	other atoms	D_e (kcal/mol)
BS04	LANL2DZ & Couty-Hall 6p & f	LANL2DZ ECP	LANL2DZ & dp	27.63
BS05	LANL2DZ & Couty-Hall 6p & f	LANL2DZ ECP	cc-pVTZ	27.42
BS06	QZVPP	LANL2DZ ECP	6-311++G(3df,3pd)	27.77
BS17	Stuttgart RSC 1997 & 2f1g	Stuttgart RSC 1997 ECP	Stuttgart RLC ECP	27.14
BS18	ZORA TZ2P all-electron	ZORA TZ2P all-electron	ZORA TZ2P all-electron	27.75
BS20	Stuttgart RSC 1997 & 2f1g	Stuttgart RSC 1997 ECP	cc-pVTZ	27.65
BS21	Stuttgart RSC 1997 & 2f1g	Stuttgart RSC 1997 ECP	aug-cc-pVTZ	27.50
BS22	Stuttgart RSC 1997 & 2f1g	Stuttgart RSC 1997 ECP	cc-pVQZ	27.87

various qualities were selected including Hay-Wadt LANL2DZ,[11] triple-ζ valence with two polarization functions (TZVPP),[12] quadruple-ζ valence with two polarization functions (QZVPP),[12] and double-ζ level Stuttgart relativistic small core (RSC) 1997.[13,14] The notation & Couty-Hall 6p indicates that a set of optimized 6p orbitals[15] were added, & f indicates that one f-polarization function[16] was added, and & 2f1g indicates that two f and one g functions[17] were added. For the inner 60 electrons of Re, LANL2DZ ECP[11] and Stuttgart RSC 1997 ECP[13] were used. For the other atoms, two types of ECP basis sets, LANL2DZ[11,18] and Stuttgart relativistic large core (RLC),[19] and three types of all-electron basis sets, correlation consistent polarized valence triple-ζ (cc-pVTZ),[20] 6-311G,[21] and 6-311++G(3df,3pd),[21,22] were selected for comparison. The notation & dp indicates that one polarization and one diffuse function[23] were added to the LANL2DZ basis sets. For the basis sets using LANL2DZ or Stuttgart settings, the Dunning double-ζ (D95V)[24] basis set was used for all H atoms. BS18 and BS19 were optimized all-electron Slater-type triple-ζ basis sets with two polarization functions (TZ2P)[25] and quadruple-ζ basis sets with four polarization functions (QZ4P)[25] for use in the zeroth-order regular approximate relativistic equation (ZORA), which were provided in the ADF program package.

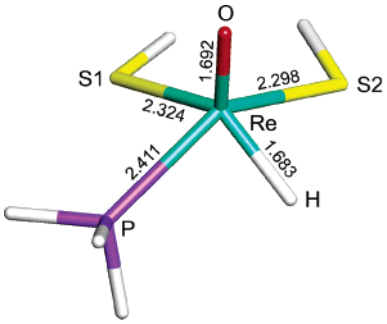

Figure 11. The geometry structure of $HReO(SH)_2-PH_3$, optimized by using PBE functional with BS20.

The dissociation energies obtained from B3LYP calculation with different basis sets in Table 1 are quite similar. There are no obvious patterns in the differences between all-electron and the two ECP basis sets. Comparing the D_e results obtained with BS01−BS04 and BS06 and BS07, we find that the effect of polarization and diffuse functions is not particularly significant. The difference between the maximum D_e (33.77 kcal/mol, BS06) and the minimum D_e (30.52 kcal/mol, BS19) is only 3.25 kcal/mol. There appears to be a trend toward small basis sets predicting larger D_e. This small difference may be due to the neglect of basis set superposition error (BSSE) corrections. On the basis of these results, we can confidently choose for further calculations a rather small basis set, BS17, to reduce computational cost dramatically without loss of precision.

Effect of Density Functional. To examine the effect of different density functionals on D_e, ten of the most popular density functionals, PW91,[26] PBE,[27] PBE1PBE,[27] OPBE,[27,28] OLYP,[28,29] BLYP,[29,30] B3LYP,[8] B3PW91,[26] BHandHLYP,[29,30] and MPW91PW91,[26,31] were selected for calculation with BS17. The calculated D_e results obtained from these different density functionals spread over a wider range (Table 2). The maximum D_e (40.89 kcal/mol, PBE1PBE) is 17.47 kcal/mol larger than the minimum D_e (23.42 kcal/mol, OLYP). Thus, it is very important to determine which functional is most suitable for calculating the Re−X bond strength for this oxorhenium molecular system.

Because no experimental value of the Re−P D_e for the system is available, the only criterion to determine an appropriate density functional is comparison to the results of a high accuracy ab initio

(9) Frisch, M. J.; et al. *Gaussian 03*, revision B.04; Gaussian, Inc.: Pittsburgh, PA, 2003; http://www.gaussian.com/.
(10) The ADF, version 2005.01, package of programs for first-principles electronic structure calculations. Baerends, E. J.; et al. *Scientific Computing & Modelling*; Amsterdam, Netherlands, 2005; http://www.scm.com/.
(11) Hay, P. J.; Wadt, W. R. *J. Chem. Phys.* **1985**, *82*, 270−283.
(12) Weigend, F.; Ahlrichs, R. *Phys. Chem. Chem. Phys.* **2005**, *7*, 3297−3305.
(13) Andrae, D.; Haeussermann, U.; Dolg, M.; Stoll, H.; Preuss, H. *Theor. Chim. Acta* **1990**, *77*, 123−141.
(14) Basis sets were obtained from the Extensible Computational Chemistry Environment Basis Set Database, version 02/25/04, as developed and distributed by the Molecular Science Computing Facility, Environmental and Molecular Sciences Laboratory, which is part of the Pacific Northwest Laboratory, P.O. Box 999, Richland, WA 99352, and funded by the U.S. Department of Energy. The Pacific Northwest Laboratory is a multiprogram laboratory operated by Battelle Memorial Institute for the U.S. Department of Energy under contract DE-AC06-76.RLO 1830. Contact Karen Schuchardt for further information. http://www.emsl.pnl.gov/forms/basisform-.html.
(15) Couty, M.; Hall, M. B. *J. Comput. Chem.* **1996**, *17*, 1359−1370.
(16) Ehlers, A. W.; Böhme, M.; Dapprich, S.; Gobbi, A.; Höllwarth, A.; Jonas, V.; Köhler, K. F.; Stegmann, R.; Veldkamp, A.; Frenking, G. *Chem. Phys. Lett.* **1993**, *208*, 111−114.
(17) Martin, J. M. L.; Sundermann, A. *J. Chem. Phys.* **2001**, *114*, 3408.
(18) (a) Dunning, T. H., Jr.; Hay, P. J. In *Methods of Electronic Structure Theory*; Schaefer, H. F., III, Ed.; Plenum Press: New York, 1977; Vol. 2. (b) Wadt, W. R.; Hay, P. J. *J. Chem. Phys.* **1985**, *82*, 284−298. (c) Hay, P. J.; Wadt, W. R. *J. Chem. Phys.* **1985**, *82*, 299−310.
(19) Bergner, A.; Dolg, M.; Kuechle, W.; Stoll, H.; Preuss, H. *Mol. Phys.* **1993**, *80*, 1431.
(20) (a) Dunning, T. H., Jr. *J. Chem. Phys.* **1989**, *90*, 1007. (b) Woon, D.; Dunning, T. H., Jr. *J. Chem. Phys.* **1993**, *98*, 1358.
(21) (a) Krishnan, R.; Binkley, J. S.; Seeger, R.; Pople, J. A. *J. Chem. Phys.* **1980**, *72*, 650. (b) McLean, A. D.; Chandler, G. S. *J. Chem. Phys.* **1980**, *72*, 5639.
(22) (a) Clark, T.; Chandrasekhar, J.; Spitznagel, G. W.; Schleyer, P. von R. *J. Comput. Chem.* **1983**, *4*, 294. (b) Gill, P. M. W.; Johnson, B. G.; Pople, J. A.; Frisch, M. J. *Chem. Phys. Lett.* **1992**, *197*, 499. (c) Frisch, M. J.; Pople, J. A.; Binkley, J. S. *J. Chem. Phys.* **1984**, *80*, 3265.
(23) Check, C. E.; Faust, T. O.; Bailey, J. M.; Wright, B. J.; Gilbert, T. M.; Sunderlin, L. S. *J. Phys. Chem. A* **2001**, *105*, 8111.
(24) Dunning, T. H., Jr.; Hay, P. J. In *Modern Theoretical Chemistry*; Schaefer, H. F., III, Ed.; Plenum Press: New York, 1976; Vol. 3, pp 1−28.
(25) Van Lenthe, E.; Baerends, E. J. *J. Comput. Chem.* **2003**, *24*, 1142−1156.
(26) (a) Burke, K.; Perdew, J. P.; Wang, Y. In *Electronic Density Functional Theory: Recent Progress and New Directions*; Dobson, J. F., Vignale, G., Das, M. P., Eds.; Plenum: New York, 1998; pp 81−111. (b) Perdew, J. P. In *Electronic Structure of Solids '91*; Ziesche, P., Eschrig, H., Eds.; Akademie Verlag: Berlin, 1991; p 11. (c) Perdew, J. P.; Chevary, J. A.; Vosko, S. H.; Jackson, K. A.; Pederson, M. R.; Singh, D. J.; Fiolhais, C. *Phys. Rev. B* **1992**, *46*, 6671−6687. (d) Perdew, J. P.; Chevary, J. A.; Vosko, S. H.; Jackson, K. A.; Pederson, M. R.; Singh, D. J.; Fiolhais, C. *Phys. Rev. B* **1993**, *48*, 4978. (e) Perdew, J. P.; Burke, K.; Wang, Y. *Phys. Rev. B* **1996**, *54*, 16533−16539.
(27) (a) Perdew, J. P.; Burke, K.; Ernzerhof, M. *Phys. Rev. Lett.* **1996**, *77*, 3865−3868. (b) Perdew, J. P.; Burke, K.; Ernzerhof, M. *Phys. Rev. Lett.* **1997**, *78*, 1396.
(28) Handy, N. C.; Cohen, A. J. *Mol. Phys.* **2001**, *99*, 403412.
(29) Lee, C.; Yang, W.; Parr, R. G. *Phys. Rev. B* **1988**, *37*, 785−789.
(30) Becke, A. D. *Phys. Rev. A* **1988**, *38*, 3098.
(31) Adamo, C.; Barone, V. *J. Chem. Phys.* **1998**, *108*, 664−675.

Table 4. Calculated Dissociation Energies between $HReO(SH)_2$ and PH_3 with BS20 and Various Methods

method[a]	D_e (kcal/mol)
PW91	27.49
PBE	27.65
PBE1PBE	30.08
OPBE	23.37
OLYP	17.16
BLYP	18.47
B3LYP	21.17
B3PW91	27.33
BHandHLYP	20.66
MPW91PW91	26.14
CCSD(T)/PBE[b]	28.27
CCSD(T)/B3LYP[c]	28.31

[a] DFT calculations optimize structures separately. [b] CCSD(T) single point energy calculation with PBE optimized structures. [c] CCSD(T) single point energy calculation with B3LYP optimized structures.

wavefunction method. Thus, we performed benchmark CCSD(T)[32] calculations with rather large basis sets (BS20) for the D_e of a similar but much simpler molecular system $HReO(SH)_2-PH_3$ by using the MOLPRO[33] ab initio program package version 2002.6. At first, we calculated the D_e between $HReO(SH)_2$ and PH_3 with various basis sets and density functionals to see if the theoretical results on this molecular system were similar to those of the large model. Next, using the geometry structures optimized by PBE (see Figure 11) and B3LYP with BS20, CCSD(T) single point energy calculations were performed in the same basis sets. The results are displayed in Tables 3 and 4.

These results indicate that the calculated dissociation energies of $HReO(SH)_2-PH_3$ also are not sensitive to basis sets but do depend on density functionals. In Table 4, the PBE and B3LYP results differ by about 6 kcal/mol difference, but the difference between the CCSD(T) single point calculations using PBE and B3LYP structures is less than 0.1 kcal/mol. This means PBE and B3LYP calculations obtain very similar geometric structures. Among all of these density functionals, the PBE, PW91, and B3PW91 have similar results and are close to the high accuracy CCSD(T) results. On the basis of all of these comparisons, we finally chose BS17 basis set and the PBE pure density functional for our further study of the ligand substitution reaction mechanisms of the oxorhenium dithiolate complexes. This combination of basis set and density functional can reduce the computational cost dramatically without lose of precision. Calculating the harmonic vibrational frequencies and noting the number of imaginary frequencies confirmed the nature of all intermediates (no imaginary frequency) and transition state structures (one imaginary frequency), which also were confirmed to connect reactants and products by the intrinsic reaction coordinate (IRC) calculations. All figures in this paper were drawn by using the JIMP2[34] molecular visualizing and manipulating program. The zero-point energy and entropic contribution have been estimated within the harmonic potential approximation. The counterpoise method, in which M, X, and Y were specified as three fragments, was use to correct the BSSE in further calculations. As a final comment, when done with careful characterizations of the computed transition states, computational chemistry will only find microscopically reversible pathways because the correct physics is built into the methodology.

Acknowledgment. This work was supported by grants from the NSF (CHE-0518074 and DMS-0216275) and The Welch Foundation (A0648). We appreciate constructive discussion with Dr. Chad Beddie (Texas A&M University, Texas).

Supporting Information Available: Absolute energies and the atomic coordinates of optimized stationary points and transition states. Complete refs 9, 10, and 33. This material is available free of charge via the Internet at http://pubs.acs.org.

JA065428Y

(32) Schütz, M. *J. Chem. Phys.* **2000**, *113*, 9986.
(33) Werner, H.-J.; et al. *MOLPRO, a package of ab initio programs, version 2002.6*; University College Cardiff Consultants, Cardiff, Wales, UK, 2003; http://www.molpro.net/.
(34) JIMP2, version 0.091, a program for visualizing and manipulating molecules: Manson, J.; Webster, C. E.; Hall, M. B. Texas A&M University, College Station, TX, 2006; http://www.chem.tamu.edu/jimp2/index.html.